Self-Regulating VO2 Photonic Pigments

Maria Letizia de Marco, Olivier Smith, Fanny Thorimbert, Cédric Boissière, Lionel Nicole, Jean-Marc Krafft, Clement Sanchez, Marco Faustini

Self-Regulating VO$_2$ Photonic Pigments

Maria Letizia De Marco, Olivier Smith, Fanny Thorimbert, Cédric Boissière, Lionel Nicole, Jean-Marc Krafft, Clement Sanchez, and Marco Faustini*

1. INTRODUCTION

Since prehistoric times, pigments have been playing a fundamental role in art, design, and industry, given their ability to enhance aesthetics and vibrancy in various surfaces and materials.[1] Conventional pigments rely on selective absorption of specific wavelengths of light to produce the perception of color. In contrast, photonic pigments derive their vibrant colors from the periodic organization of nanostructures within the material, which behaves as a diffraction grating for visible wavelengths.[2] Structural colors manifest in numerous natural and synthetic materials, including avian plumage and butterfly wings,[3,4] and leverage the manipulation of light to produce an array of hues that are resistant to fading or color change. This unique feature has earned photonic pigments tremendous appeal across an extensive range of applications, including textiles, cosmetics, and architecture. Structurally colored pigments have been prepared from colloidal polymers,[5] cellulose,[6] block-copolymers,[7,8] or other inorganic materials[9] such as metallic resonators[10] or MOFs.[11,12] One emerging challenge in the field consists of integrating additional functionalities to the pigments beyond color. For instance, temperature-[13] or stress-responsive photonic pigments[14] have been recently reported. Interestingly, temperature-responsive microporous ZIF-8 photonic balls,[11] or periodic arrays of mesoporous TiO$_2$,[15] have been used as local thermal probes in the presence of vapors.[16] All these examples concern the fabrication of pigments acting as sensors in which the applications of *stimuli* (temperature, solvent, and stress) results in a color change. A less explored aspect consists of integrating autonomous light and thermal regulation capabilities to the photonic pigments. For instance, integrating phase changing materials would enable the emergence of a new generation of self-regulating photonic pigments that modulate autonomously the flow of light in the infrared range (IR), while conserving their structural color in the visible range.[17] In this

context, vanadium di-oxide (VO_2) is the most promising material for thermo-regulation. VO_2 exhibits a phase transition from a monoclinic insulating phase ($P2_1/c$) to a rutile phase ($P4_2/mnm$) with metallic properties.[18] The phase transition typically occurs at 340 K (67 °C). In the low temperature monoclinic phase, V atoms are paired in V−V dimers, forming a zig-zag structure along the c-axis, with the V−V distance being alternatively 2.65 and 3.12 Å. Upon heating above the transition temperature, the V atoms line up along the c-axis with a regular V−V distance of 2.87 Å, causing the overlap among the bonding $d_\parallel$ and anti-bonding π^* bands to form the rutile conduction band.[17,19−22] The phase transition causes dramatic change in VO_2 resistivity[23,24] and optical properties in the infrared range.[25−27] Namely, a decrease of IR transmittance is observed in the high temperature rutile phase, due to its metallic nature. The optical switching property has a great technological potential for the realization of self-regulating smart coatings for energy saving applications, as it enables the dynamic control of sun-light heating by reducing IR radiation above the transition temperature.[18,28−30] Typically, VO_2-based smart coatings are realized by atomic layer deposition,[31] chemical layer deposition,[29,32,33] sputtering,[30,34,35] and vanadium film oxidation.[36,37] These techniques allow to successfully and reproducibly obtain VO_2 thin films with self-regulating properties in the IR, but their application is limited to few rigid substrates (glass, ITO, quartz, and sapphire)[31,36,37] and does not allow for easy structuration of the materials. In addition, VO_2 coatings typically exhibit a yellow-brownish color,[30,38] which might be considered anesthetic for smart window applications. A fabrication process enabling direct VO_2 structuration with a periodic architecture at the nanoscale is required in order to introduce a structural color in VO_2 self-regulating materials. Here, we present a robust and scalable templated soft-chemistry approach for the high-throughput fabrication of VO_2 self-regulating photonic pigments with a periodic architecture.

Pigments are fabricated by a templated sol−gel route using the spray-drying process followed by thermal annealing. The sol−gel synthesis enables precise control on both chemistry and structuration,[39,40] and it has been previously applied to the synthesis of VO_2 thin films with switching IR optical properties[24,41−43] as well as porous materials.[44] Despite these examples, it is well known that synthetizing and shaping stable VO_2-based materials in a reliable way and at large scale (gram-scale) represents a longstanding challenge in the domain.[30] To overcome this issue, we optimized the thermal annealing process to obtain single phase VO_2 pigments based on the pseudomorphic transformation between V_2O_3 and VO_2 by controlled oxidation. The versatility of the whole process (templated sol−gel + thermal annealing) allows for the tuning of pore size and spacing, enabling production of green, yellow, and red VO_2 pigments. *In situ* thermal hyperspectral microscopy and IR transmittance spectroscopy enable analysis of VO_2 pigments optical properties evolution as a function of the temperature. Because of the inherent properties of VO_2, the IR transmittance decreases upon the phase transition, while the structural color in the visible range remains unaltered.[45] Finally, we also demonstrate that such pigments can be easily integrated into paints and coating or embedded into elastomeric objects opening interesting perspectives for applications in textile or architecture.

2. RESULTS

The general concept of self-regulating photonic pigments is illustrated in Figure 1. The materials are micrometric spheres
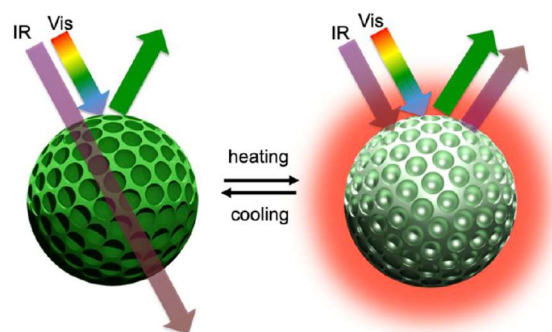

Figure 1. Scheme of the photonic VO_2 pigments exhibiting thermo-optical self-regulation: the particles have a structural color resulting from ordered macro-porosity. Above the transition temperature, the particles have metallic properties and reduce IR transmission while their color in the visible range is not affected.

composed of VO_2 with an inverse opal structure, as displayed in Figure 2. The spheres are polydisperse in size as expected by spray-drying process (Figure 2A). Their ordered, monodisperse porosity (see Figure 2B,C) leads to a specific structural color in the visible range, which depends on the pore morphology (size, distance, local or extended order) and on the refractive index of the matrix. The visible structural color is not expected to change upon phase transition, since the refractive index of VO_2 in the visible range does not change between the monoclinic and rutile phase of VO_2.[45] Instead, above the transition temperature, the IR transmittance of VO_2 pigments is expected to decrease, enabling autonomous regulation of the IR radiation heating while maintaining their structural color in the visible range.

2.1. Fabrication Process of Macroporous Ordered VO_2 Photonic Pigments. The porous photonic VO_2 particles were produced *via* the sol−gel process using a templated spray-drying process. The liquid precursor vanadium (V) oxy-triisopropoxide (VTIP, $VO(C_3H_8O)_3$) was used as a molecular precursor for the VO_2 particles. VTIP (500 mg) was added to 50 g of MilliQ water under magnetic stirring. VTIP hydrolyzes fast when in contact with water, forming dark orange precipitates, which redissolve after 5 min under magnetic stirring, yielding an orange, clear solution. When the VTIP was fully hydrolyzed, a water suspension of monodisperse polymethyl methacrylate spheres (PMMA latex) was added to the solution, either with a 1:1 or a 1:2 PMMA-to-VTIP mass ratio. The VTIP-PMMA suspension was kept under magnetic stirring and atomized using a Buchi B-290 mini spray dryer at a temperature of 200 °C, yielding a dry orange powder. This strategy combines the sol−gel chemistry with the evaporation induced self-assembly (EISA).[44,46] During spray-drying, the sol−gel reaction is confined in water droplets, which also contain suspended PMMA latex. Upon water evaporation, the PMMA particles self-assemble to form ordered superstructures (EISA) embedded in the amorphous matrix formed by the precipitation and polycondensation of the hydrolyzed VTIP precursor during the sol−gel reaction inside the droplet (Figure 3B,E). This process enables fine control on the chemistry *via* the sol−gel reactivity, as well as on the
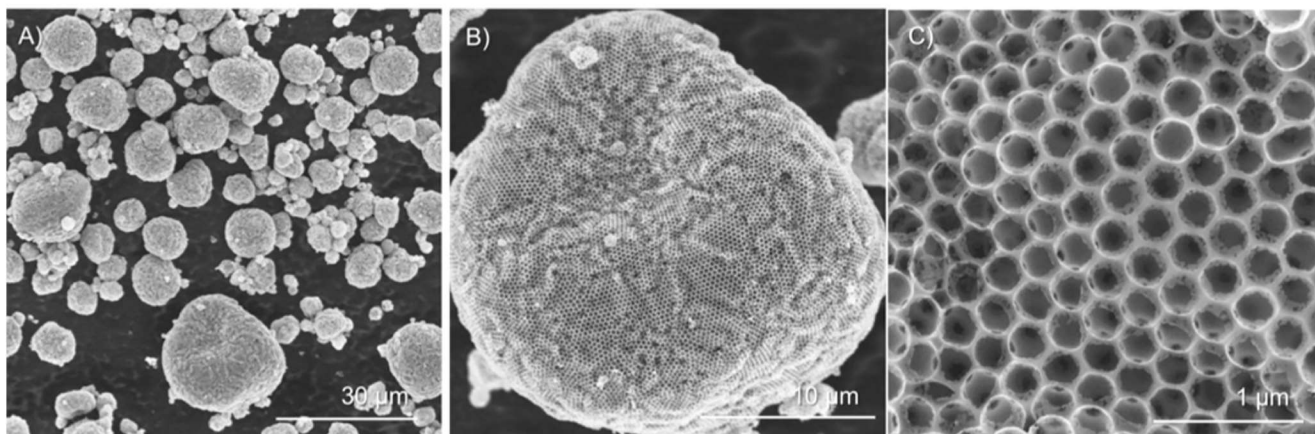
Figure 2. SEM micrograph of the typical photonic VO$_2$ pigments at different magnifications.
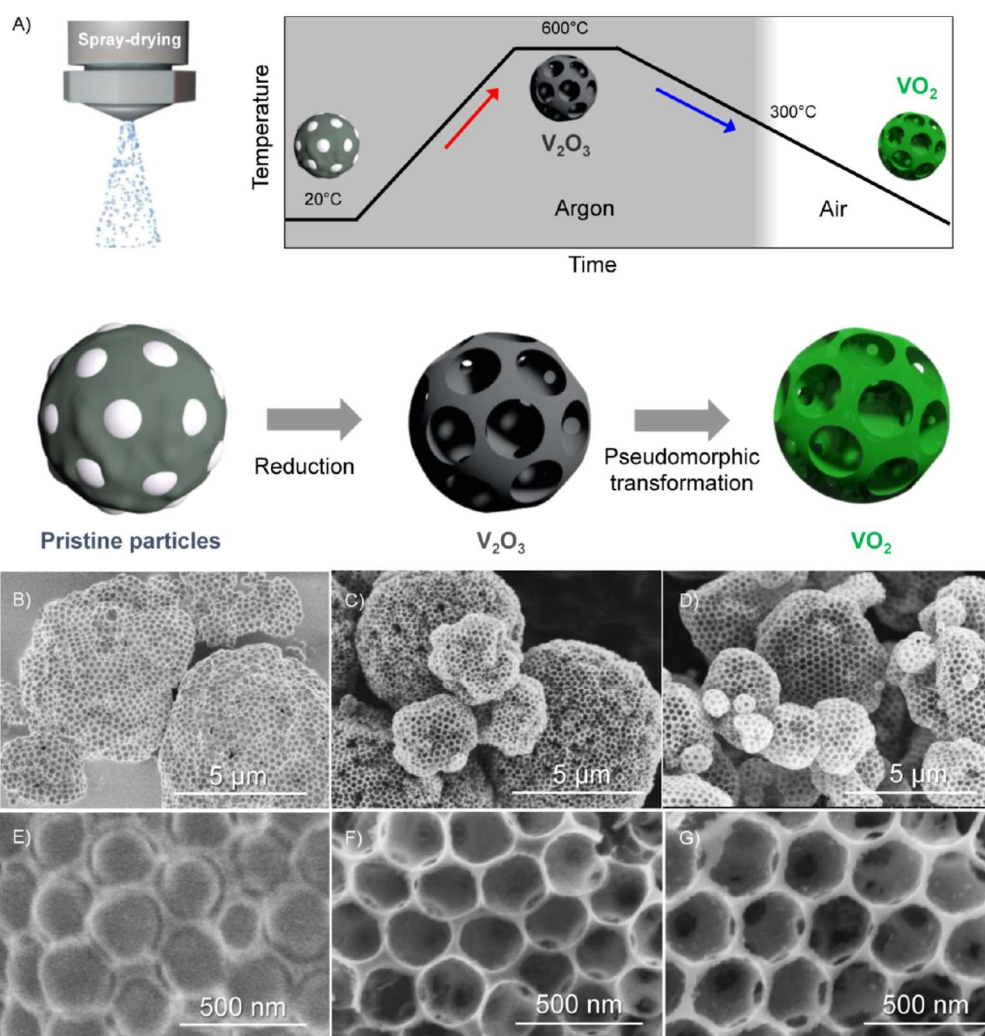

Figure 3. Synthesis of porous VO$_2$ particles by templated spray-drying, followed by annealing under a controlled atmosphere. Scheme of the spray-drying and annealing process (A). Scanning electron microscopy (SEM) pictures of pristine as-sprayed particles (B,E), of porous V$_2$O$_3$ (C,F) and of porous VO$_2$ (D,G) obtained for different phases of the annealing process.

structuration of the particles *via* the use of templating PMMA agents. Moreover, it allows for gram-scale production of dry powders, ready for annealing, without the need for further purification. The as-sprayed pristine particles were initially annealed in a tubular oven at 600 °C under a flow of argon. Thermal annealing causes PMMA decomposition as well as the reduction and crystallization of the amorphous matrix, yielding pure V$_2$O$_3$ particles characterized by an inverse opal structure, with the pores organized in a compact hexagonal lattice (Figures 3C,F and 4C). Surprisingly, starting from a molecular
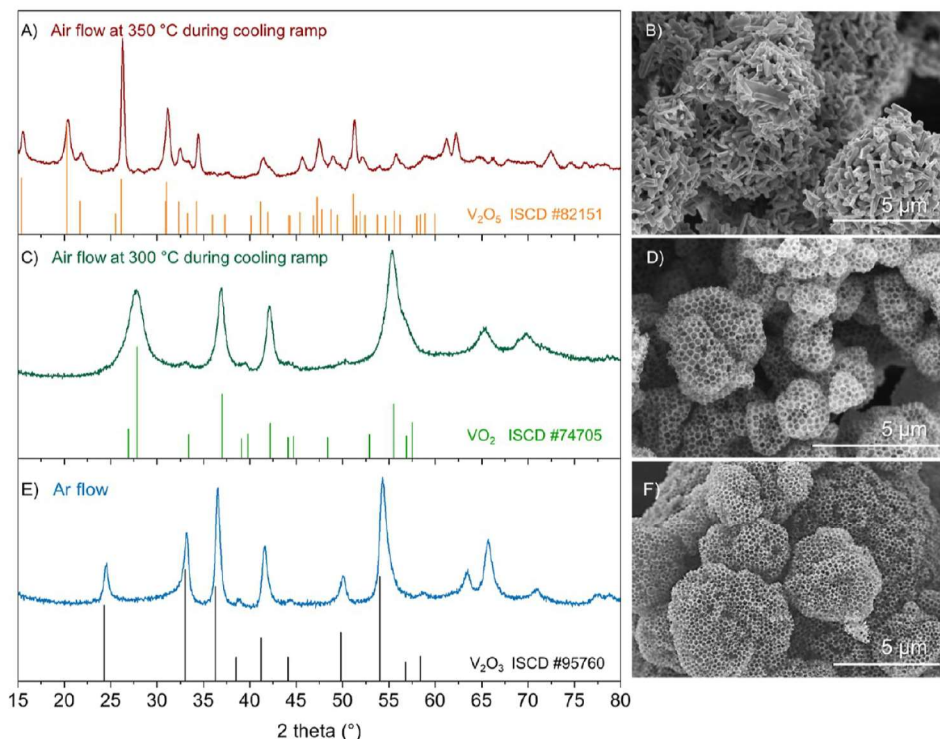
Figure 4. Thermal treatment in the tubular oven. XRD patterns (A,C,E) and corresponding SEM micrographs (B,D,F) of templated particles annealed under Ar at 600 °C, when they cool down under Ar [V_2O_3, (E,F)], when they cool down under air once the oven temperature descended below 300 °C [VO_2, (C,D)], and when they cool down under air once when the oven temperature descended below 350 °C [V_2O_5, (A,B)]. Each phase has been identified thanks to the reference patterns available in the ISCD database.

precursor with the vanadium centre in the oxidation state (V), a pure V(III) oxide phase is obtained upon annealing at 600 °C under Ar. This behavior is probably due to the reducing activity of the PMMA latex template under an inert atmosphere. In order to stabilize the formation of pure VO_2, where the vanadium has oxidation number (IV), we initially explored the effect of the annealing temperature and O_2 partial pressure on the oxide phase, following the Ellingham diagram for vanadium oxides.[47] According to the Ellingham diagram, the VO_2 phase can be stabilized either by decreasing the annealing temperature, or by increasing the oxygen partial pressure at a given temperature. By decreasing the annealing temperature, we obtained pure V_2O_3 (500 °C) or a mix of V_2O_3 and V_2O_5 (450 °C), as reported in Figure S1 in Supporting Information. Gradually increasing the O_2 partial pressure at 600 °C only produced pure V_2O_5 (for O_2 volume concentration above 1%) or pure V_2O_3 (for O_2 concentration below 1%), as shown in Figure S2 in the Supporting Information. Since stabilizing pure VO_2 by direct annealing of pristine particles was difficult, we explored a two-step approach, involving the pseudomorphic transformation of V_2O_3 into VO_2 by controlled post-annealing oxidation.

Pure porous VO_2 particles in the monoclinic phase ($P2_1/c$) can be obtained by treating porous V_2O_3 particles at 350 °C for 5 min in a muffle furnace under static air. The onset of V_2O_3 oxidation to VO_2 is observed around 330 °C, while above 370 °C the oxidation to V_2O_5 begins (see Figure S3 in the Supporting Information). We further optimized this process by switching the gas flow from pure Ar to air during the cooling ramp directly inside the tubular oven, in order to eliminate the second step in the muffle furnace (see the scheme in Figure 3A).

Initially, we tested 350 °C as limit temperature to introduce air in the tubular oven. However, these conditions proved to be too oxidizing, and pure V_2O_5 is obtained (Figure 4A). The porous morphology is lost when V_2O_3 is oxidized to V_2O_5, due to the excessive growth of the crystallites (Figure 4B). Pure VO_2 particles were stabilized by introducing air when the oven temperature decreased below 300 °C during the cooling ramp, and leaving the system spontaneously cool for 1 h (Figure 4C). In this way, we succeeded to exploit the residual heat from the tubular oven for V_2O_3 oxidation without implementing a second annealing step. For both the one-step and two-step V_2O_3 oxidation processes, a pseudomorphic transformation occurs, where the ordered porous structure of V_2O_3 is preserved upon oxidation to VO_2 (see Figures 2, 3F,G and 4D,F). This pseudomorphic V_2O_3 to VO_2 transformation probably involves a topotactic oxidation similar to what reported by Yamaguchi *et al.* for VO_2 epitaxial films.[47]

The transmission electron microscopy (TEM) characterization of the VO_2 particles reveals that the pores walls are composed by VO_2 elongated nanocrystallites, whose (011) planes are aligned along the pore edges (Figure 5).

The orientation of the crystallites along pore walls suggests that the PMMA template impresses a direction of growth for the VO_2 crystallites during oxidation of V_2O_3 and is probably responsible for the phase selectivity of the pseudomorphic transformation. In order to further investigate the role played by the PMMA for structuration and phase selectivity, we produced reference non-templated particles by spray-drying an aqueous solution of VTIP. Thermal annealing of these reference particles at 600 °C under air yielded a mixture of many different phases, including V_2O_5, VO_2, and V_2O_3, rather than pure V_2O_3 (see Figure S4). Therefore, it is impossible to
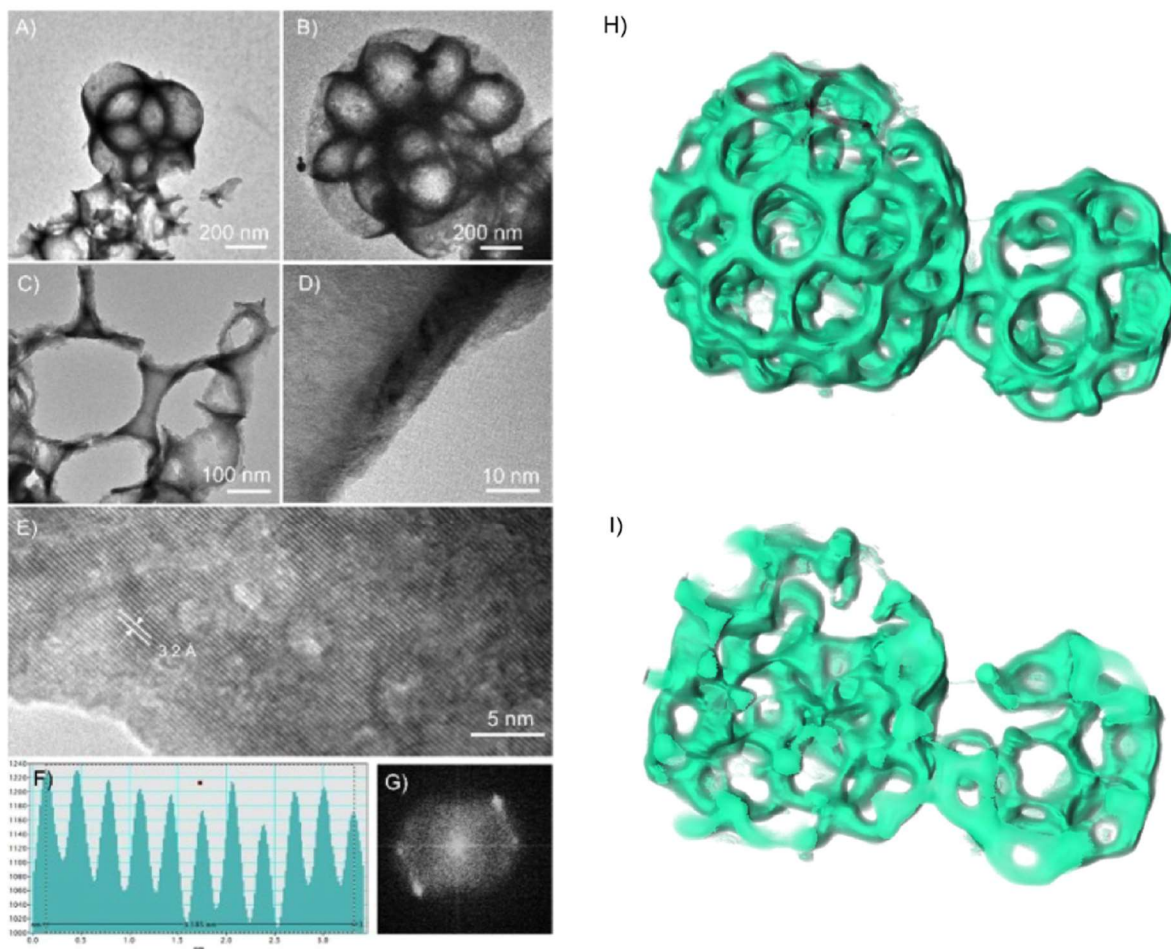
Figure 5. Transmission electron microscopy (TEM) characterization of VO$_2$ porous particles. VO$_2$ particles synthetized using 360 (A) and 500 nm (B) PMMA latex particles. Details of the porous structure showing that the crystallites are aligned along the pore walls (C,D). High resolution TEM image of a pore wall showing the crystalline lattice with interplanar distance 3.2 Å (E), corresponding to the (011) planes of monoclinic VO$_2$, as confirmed by the intensity histogram (F) and by the simulated Fast Fourier Transform (FFT) (G). Electron tomographic reconstruction (H) and cross-section (I) of two porous VO$_2$ particles.

convert these powders to pure VO$_2$ by pseudomorphic transformation, contrarily to what observed with the porous particles. This suggests that here the PMMA latex is not simply a sacrificial template for inducing structuration, but plays a key chemical role for ensuring phase selectivity. Previous works from our group have shown that under an inert atmosphere, PMMA acts both as a templating and as a reducing agent,[48,49] which explains why a pure V$_2$O$_3$ phase is obtained only for templated particles. In summary, pure monoclinic VO$_2$ ($P2_1/c$) could be obtained only by pseudomorphic transformation with a controlled re-oxidation of the porous V$_2$O$_3$ particles, due to the important role played by PMMA in this process.

2.2. Optical Properties of VO$_2$ Photonic Inks. The inner structure of two small VO$_2$ porous particles was further characterized by electron tomography, as displayed in Figure 5G,H; the analysis confirms that the pigments present an inverse opal structure. In ordered inverse opal structures, the size of the pores, as well as their distance, is expected to affect the structural color, since these parameters affect the lattice parameter of photonic crystals and therefore the position of the photonic stop band.[50] The spray-drying protocol allows to easily tune the size of the pores, by changing the size of the template PMMA particles, without affecting the crystalline phase of the VO$_2$ particles (see Figures 5A,B and S5). Here, we

tuned the lattice parameter by playing both with the size of the pores and the filling factor, *i.e.,* the volume fraction occupied by the pores compared to the volume fraction of the surrounding VO$_2$ phase.[51] The different structural colors resulting from different pore size and filling factor have been characterized using hyperspectral microscopy. Hyperspectral microscopy acquires information across the visible spectra and combines them into a hyperspectral image. The microscope is equipped with a spectrometer and a piezoelectric scanner, which moves the samples in the x and y directions in order to collect spectra of a selected sample area. Each pixel of the reconstructed hyperspectral image is associated to its reflection spectrum.[15]

The hyperspectral setup is also equipped with a camera for conventional optical microscopy imaging. Figure 6 shows an overview of the photonic lattice of different VO$_2$ pigments and their resulting structural colors characterized by hyperspectral and optical microscopy. VO$_2$ particles realized using 360 nm PMMA (Figure 6A) exhibit a vivid green color as determined by optical (Figure 6B) and hyperspectral images (Figure 6C). The reflectance peak of three particles from this batch ranges between ~500 and ~530 nm, in good agreement with hyperspectral and optical images (Figure 6D). By increasing the PMMA template size to 500 nm (Figure 6E), the reflection peak red-shifts to ~600 nm (Figure 6H), resulting in yellow
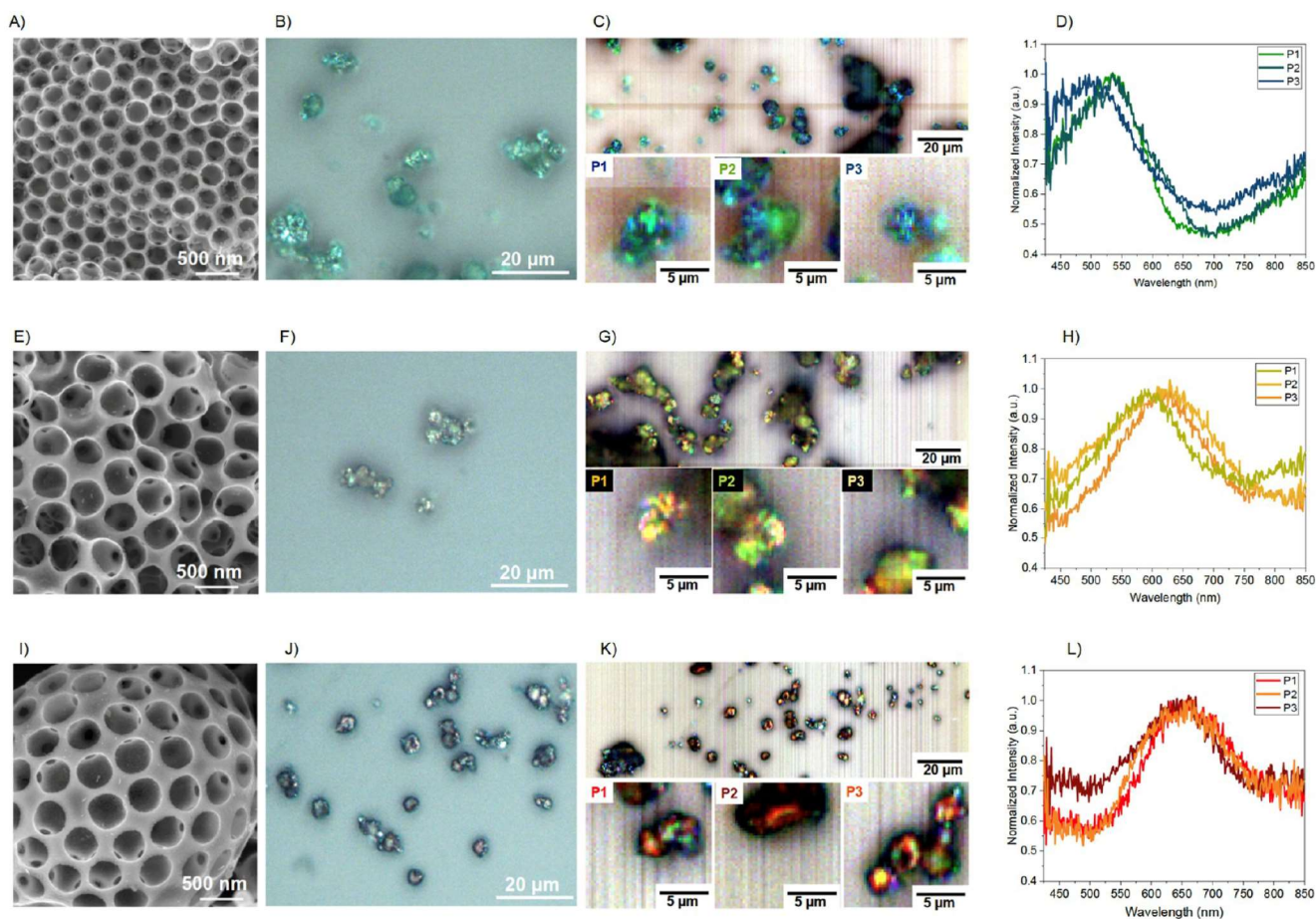
Figure 6. Structural color of photonic VO$_2$ particles as a function of pore size and pore spacing. SEM pictures (A,E,I), optical images (B,F,J), hyperspectral images (C,G,K), and conventional normalized reflectance spectra (D,H,L) of green (A–D), yellow (E–H), and red (I–L) photonic VO$_2$ particles.
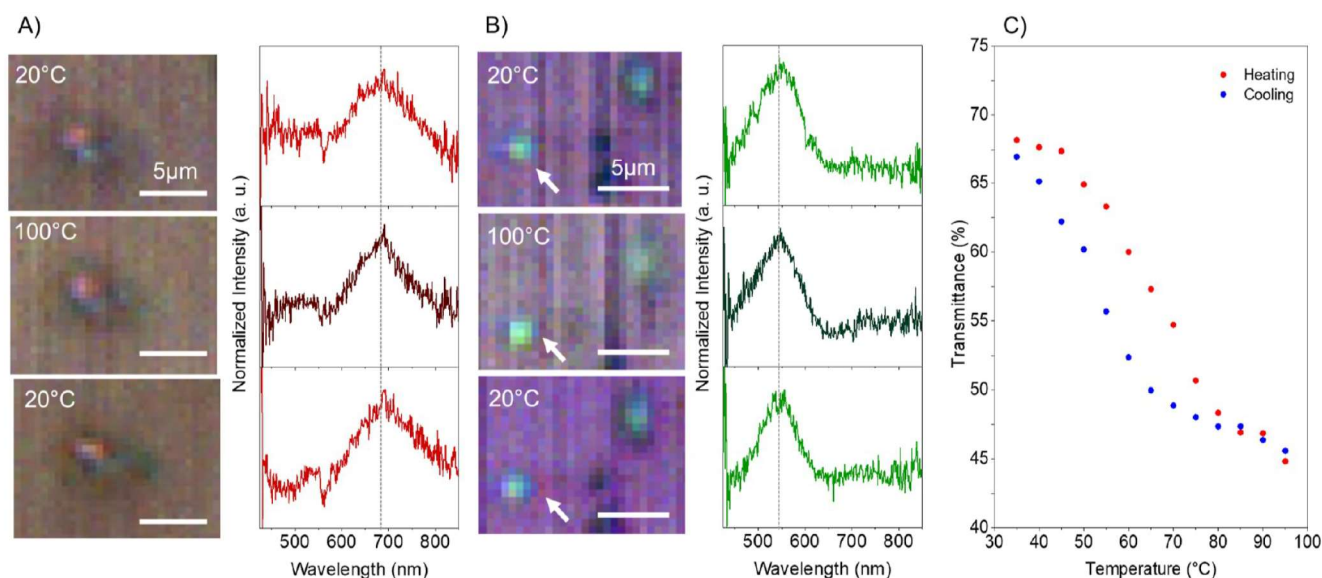
Figure 7. Evolution of the optical properties of the VO$_2$ pigments upon phase transition. Optical characterization in the visible range by *in situ* hyperspectral microscopy for red (A) and green (B) VO$_2$ pigments. The line across the peaks serves as a guide for the eye. (C) Evolution of the transmittance at 4000 cm^{-1} as a function of the temperature by *in situ* IR transmission spectroscopy.

VO$_2$ particles (Figure 6 F, G). The red structural color was also obtained with the 500 nm PMMA particles, by halving their

concentration with respect to the VTIP in the precursor solution. This caused the wall thickness to increase due to a

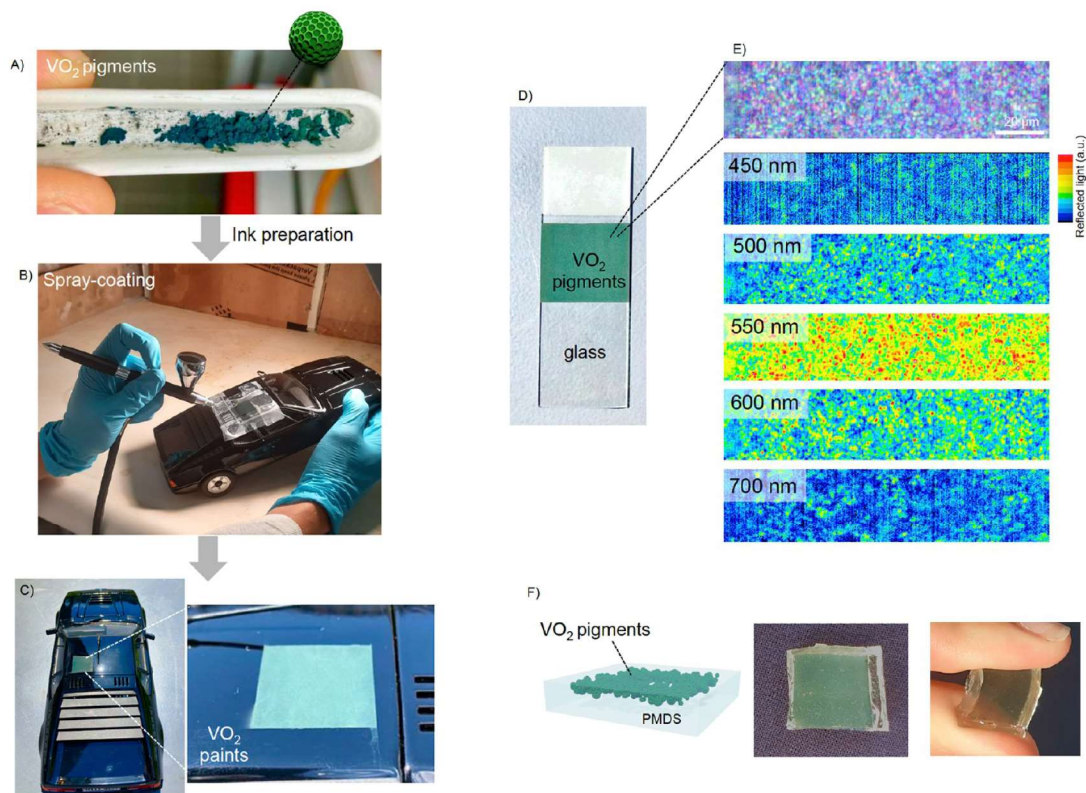**Figure 8.** Photographs of the VO₂ photonic powder (A), spray-coating process (B) and model car coated by the VO₂ photonic paint (C). Photograph (D) and spectral mapping (E) obtained by hyperspectral microscopy of a VO₂-coated glass slide. Illustration and photographs of the VO₂ pigments embedded in PDMS (F).

lower filling factor, resulting in both lattice parameter and effective refractive index increase (Figure 6I), with a consequent red-shift of the reflection peak to ∼650−700 nm, resulting in photonic red particles (Figure 6J,K).

2.3. Phase Transition Behavior of VO₂ Self-Regulating Photonic Pigments. The phase transition behavior of the photonic VO₂ particles was measured first in the state of powders by differential scanning calorimetry (DSC) and *in situ* IR diffuse reflectance (Figure S6 in Supporting Information). The DSC curve shows the endothermic peak for insulator to metallic transition at ∼66 °C, while the exothermic peak is at about 50 °C (Figure S6A). The transition temperature and the slight hysteresis between the insulator-to-metal and metal-to-insulator transitions are typical of VO₂. Proof of phase transition is also found in the mid IR spectra of the particles; where the large band at 700 cm⁻¹, typical of V−O−V stretching modes, disappears above the transition temperature, due to the screening effect of the free electrons in the rutile conduction band. The bands at ∼930 and 1020 cm⁻¹, on the other side, do not disappear upon phase transition and are attributed to the stretching of vanadyl groups (V=O), having oxidation state +4 and +5 respectively, attributed to defects and terminal oxygens bonded on the surface.[52−56]

The phase transition was also characterized by following the evolution of the optical properties of the VO₂ pigments in the visible and IR range. The hyperspectral microscopy was used to characterize any change in the visible structural color, following phase transition, thanks to a heating platform installed on the microscope sample stage, which allows heating up and cooling down the sample in a controlled manner during

observation. Photonic "green" and "red" VO₂ particles were characterized by hyperspectral imaging at 20 °C and then heated at 100 °C at a rate of 5 °C min⁻¹. Their reflectance spectra were recorded after a dwelling time of 10 min at 100 °C. They were cooled down to 20 °C and characterized again after cooling down. The results are presented in Figure 7A,B and show that the reflectance peak does not shift upon heating, meaning that the structural color in the visible is not affected by the VO₂ phase transition from monoclinic to rutile.

In situ IR transmission spectroscopy was carried out on a thin film of "green" photonic VO₂ spray-coated onto a double-polished Si substrate, using an IR ellipsometry setup in transmission mode. A heating platform, installed on the ellipsometry set-up, allowed to increase and decrease the sample temperature in a controlled way. The sample temperature was increased to 100 °C with a rate of 5 °C min⁻¹ and then cooled back to 30 °C at the same rate. Transmittance spectra were recorded at 4000 cm⁻¹ every 5 °C (see Figure 7C). The transmittance decreases by 25% upon phase transition and increases again upon cooling, showing a hysteresis behavior typical of the semiconductor-to-metal VO₂ phase transition.

These results confirm that the VO₂ pigments efficiently screen IR radiation, while maintaining their structural color in the visible range; therefore, they are highly suitable for the realization of self-regulating photonic coatings. In fact, the advantage of these free-standing self-regulating photonic pigments is that they can be readily applied to any substrate of any shape, by scalable methods without the need for further treatment. For instance, to carry out the *in situ* IR transmission

characterization, the powders were readily coated onto a Si substrate by spray-coating. To illustrate the versatility of this approach, we produced several other examples of photonic coatings prepared by spray coating from the VO$_2$ pigments (displayed in Figure 8). We first prepared an ink by suspending the green VO$_2$ pigments (Figure 8A) in isopropanol/water. We then applied the ink by using an airbrush, which is a small, air-operated tool that atomizes and sprays paints on objects with complex geometry. As a proof of concept, we coated a 3 × 3 cm metallic surface of a black model car (Figure 8B). The resulting green coating is displayed in the photograph in Figure 8C. Green VO$_2$ based films can therefore be applied to several substrates such metal, silicon, or glass substrates.

The optical quality of VO$_2$-coated glass was probed by hyperspectral microscopy, as shown in Figure 8E. One interesting feature of this technique is that it enables spectral mapping providing important insights of structural homogeneity. The spectral mapping of the film is shown in Figure 8E. We represented here the specular reflected intensity at several wavelengths from 450 to 700 nm as function of the location in the surface. The coating presents the highest reflection at 550 nm with the more reflective zones that correspond to single VO$_2$ particles homogenously distributed in the film.

We also demonstrated that VO$_2$ photonic pigment coatings could be embedded in a polydymethyl siloxane (PDMS) matrix. This was achieved by first applying the coating on a silicon wafer and by transferring the VO$_2$ pigments by pouring the liquid PDMS before reticulation (more details in the experimental section). Importantly, as shown in Figure 8F the VO$_2$ pigments can be protected in an elastomeric flexible matrix without losing their green structural colors. The preservation of color strongly indicates that the PDMS does not entirely fill the pores; instead, it probably encapsulates the pigments. This observation is crucial because if the PDMS were to completely fill the pores, the structural color would be lost due to the reduced refractive index contrast between the VO2 walls and the surrounding medium. While preliminary, this last experiment opens many perspectives for the fabricating of self-regulating colored composite objects.

3. CONCLUSIONS

In this work, we have introduced self-regulating VO$_2$ photonic pigments, achieved by creating ordered porosity in VO$_2$ particles through a versatile PMMA-templated spray-drying route. The spray-drying process allows for the combination of sol−gel chemistry with templating synthesis enabling precise control over pore morphology. We have found that the PMMA template plays a crucial role not only in particle structuring but also in stabilizing a pure V$_2$O$_3$ phase during thermal annealing. Pure V$_2$O$_3$ porous particles can be transformed into porous VO$_2$ monoclinic particles through pseudomorphic oxidation, which can be carried out in a separate second step using a muffle furnace, or in a single step by harnessing the residual heat in the tubular oven during the cooling ramp. Complete conversion of V$_2$O$_3$ to VO$_2$ is only achievable with the porous templated particles, while a mixture of various phases is obtained for reference non-porous particles. By adjusting the size of the pores and the filling factor in the VO$_2$ matrix, we produced photonic pigments in green, yellow, and red shades. A set of *ex situ* and *in situ* techniques have been used to characterize the phase transition properties of the VO$_2$ pigments. These analyses have revealed that these pigments

maintain their color in the visible range but efficiently block light transmission in the infrared (IR) range.

For future research, two potential avenues could be explored. First, the transition temperature of the VO$_2$ phase could be reduced through doping, and second, the long-term chemical and mechanical stability of the pigments could be investigated. Furthermore, the process could be further enhanced by combining the spray-drying and calcination steps, possibly implementing a spray-pyrolysis-based approach. Nevertheless, already at this stage, we demonstrated that these self-regulating pigments can easily processed into inks and integrated into paints and coating or embedded into elastomeric objects opening intriguing perspectives for applications in textile, architecture, or beyond.

4. EXPERIMENTAL SECTION

4.1. Materials. Vanadium (V) oxytriisopropoxide (VTIP) was purchased from Sigma-Aldrich and stored in an Ar filled glovebox. The 500 nm PMMA latex suspension in water (5 mg/mL) was purchased from Alpha Nanotech and stored in a refrigerator at 4 °C. The methyl methacrylate and 2,2′-azobis(2methylpropionamide) dihydrochloride used for the synthesis of 360 nm PMMA latex particles were purchased from Sigma-Aldrich and stored in a refrigerator at 4 °C. Ultrapure water (18 MΩ·cm) used for spray drying synthesis was obtained with a MilliQ purification system.

4.2. PMMA Latex Synthesis. PMMA latex particles with a diameter of 360 nm were synthetized by emulsion radical polymerization in water, following the protocol published by Hatton *et al.*[57] The as produced PMMA latex suspension has a concentration of 13% in weight in water.

4.3. Spray-Drying Protocol. VTIP (500 mg) was dissolved in 50 g of ultrapure water (1% wt). The solution was magnetically stirred until it became transparent with an orange color. To produce photonic green VO$_2$ particles, a suspension of 360 nm PMMA was added, in order to obtain a PMMA to VTIP mass ratio of 1:1. To produce photonic yellow and red VO$_2$ pigments, a suspension of 500 nm PMMA was used, with a 1:1 and 1:2 mass ratio *vs* VTIP respectively. In every case, the VTIP-PMMA suspensions were stirred for 15 min, before being atomized using a B-290 mini spray dryer from Büchi. The nozzle temperature was set to 200 °C, the VTIP-PMMA suspension flow rate to 6 mL min^{-1}, the air flow rate to ∼8 L min^{-1}, and the pumping rate to 450 L min^{-1} (*i.e.*, 65% of the maximum pumping rate) as reported previously.[58] The as-sprayed pristine samples were stored in an oven at 50 °C before annealing.

4.4. Annealing Protocol. V$_2$O$_3$ porous particles were obtained by thermal annealing the pristine particles in a tubular oven at 600 °C under a flow of Ar (1 L min^{-1}). The heating ramp was set to 5 °C min^{-1}, and the dwell time at 600 °C was 5 min. The samples were let to cool in the tubular oven under the Ar flow. Before annealing, the tubular oven was purged with Ar for 1 h to avoid air contamination.

VO$_2$ porous particles were obtained by pseudomorphic transformation of the V$_2$O$_3$ porous particles. After annealing under Ar in the tubular oven, V$_2$O$_3$ particles were oxidized in a muffle furnace under static air at 350 °C for 5 min. To avoid oxidation to V$_2$O$_5$, after 5 min, the particles were removed from the oven to "quench" the oxidation reaction.

VO$_2$ porous particles were also obtained in a one-step process in the tubular oven. The annealing of the pristine powders was carried out at 600 °C for 5 min under a flow of Ar and with a heating rate of 5 °C min^{-1} as in the case of V$_2$O$_3$ particles. During the cooling ramp, when the oven temperature descended below 300 °C, the gas flow was switched to air. The system was allowed to cool under a flow of air for 1 h, before removing the VO$_2$ porous particles. If the gas flow was switched to air at 350 °C instead of 300 °C, pure V$_2$O$_5$ particles are obtained.

The annealing experiments under a mixed Ar-Air atmosphere were carried out, thanks to a flow-controller (SOLGEL WAY) connected to the gas supply and the tubular oven. The total gas flow was set to 1 L

min^{-1}, and the relative percentage of Air in Ar was adjusted to 0.5, 2, 5, and 10%.

4.5. Spray-Coating of Photonic Films Composed of VO$_2$ Photonic Particles. VO$_2$ photonic particles (10 mg) were dispersed in 5 g of solvent, composed of mixture of water and isopropanol (1:4 in weight). The suspension was stirred and then spray-coated on different substrates using an airbrush tool. Silicon and glass substrates were heated to 60 °C in order to facilitate solvent evaporation during the spray coating procedure.

4.6. VO$_2$ Photonic Films Embedding in a PDMS Matrix. The spray-coated films of VO$_2$ photonic particles were placed in a mold and filled with a mixture of polydimethylsiloxane (PDMS) liquid monomer and a reticulating agent in a 9:1 weight *ratio*. The mold was placed in an oven at 70 °C for 15 min to allow for PDMS reticulation.

4.7. Characterization Techniques. *4.7.1. X-ray Diffraction.* XRD characterization was carried out using a D8 Advance powder diffractometer from Bruker, equipped with a Cu anode (1.54 Å). The operating voltage and current were 40 kV and 30 mA, respectively. Powder diffractograms were collected in a 2θ range between 15 and 85°, with a 0.039° step size and an acquisition time of 2 s for each point.

4.7.2. Scanning Electron Microscopy. Powder samples were deposited on conductive carbon tape for observation. SEM imaging was performed with SU-70 Hitachi FESEM, equipped with a Schottky electron emission gun. Pristine, as-annealed particles were characterized with an accelerating voltage of 1 kV, while V$_2$O$_3$ and VO$_2$ particles were characterized with an accelerating voltage of 5 kV. The working distance was set to 7 mm.

4.7.3. Transmission Electron Microscopy. Transmission electron microscopy (TEM) measurements were carried out on an FEI Tecnai 120 microscope operated at 120 kV and equipped with a Gatan Orius 832 digital CCD numeric camera. Samples were prepared by drop-casting a suspension of VO$_2$ particles in ethanol onto 300 mesh carbon-coated copper grids.

4.7.4. Transmission Electron Tomography. Transmission electron tomography was carried out with a JEOL 2100 FEG S/TEM microscope operated at 200 kV, equipped with a spherical aberration probe corrector (Cs from CEOS), high-resolution objective lens pole piece, and an UltraScan1000 CCD array detector (GATAN). The software ImageJ was used for tomogram reconstruction (TomoJ) and 3D volume rendering (Volume Viewer).

4.7.5. Differential Scanning Calorimetry. A DSC Q20 from TA Instrument was used for differential scanning calorimetry. The temperature was cycled between 0 and 200 °C with a rate of 10 °C min^{-1} and under a flow nitrogen (50 mL min^{-1}).

4.7.6. In Situ IR Diffuse Reflectance. Diffuse reflectance infrared spectra (DRIFTS) were recorded using a Bruker Vertex 70 spectrometer equipped with a MCT detector (4 cm^{-1} resolution, 128 scans/spectrum) and a Thermo Scientific Collector II Diffuse Reflectance accessory. The powdered sample (20−40 mg) was placed inside a heated crucible located in a Thermo Spectra-Tech high temperature environmental cell equipped with two ZnSe windows. In the cell, Ar flow pass through the powdered sample.

4.7.7. Hyperspectral Microscopy. A Cytoviva hyperspectral microscope was used for the characterization of the photonic VO$_2$ particles. The powders were deposited on a glass microscopy slab and dispersed by tapping with the spatula on the glass slab. For *ex situ* characterization, a 50× objective was used in reflection bright field mode, and the acquisition time was set to 0.5 s. *In situ* characterization during phase transition was carried out in reflection, bright field mode, with a 100× objective and the acquisition time was set to 0.5 s with a 100× objective. The sample temperature was controlled with a heating platform (Linkam Scientific), which can be installed on the sample stage of the Cytoviva microscope. The heating rate was set to 5 °C min^{-1}, and the temperature was cycled from 20 to 100 °C. The samples were left equilibrating 10 min before collecting the hyperspectral images at 100 °C.

4.7.8. In Situ IR Transmittance. The variation of IR transmittance as a function of the temperature was measured on thin films composed of VO$_2$ photonic particles spray-dried onto double polished Si substrates (transparent to the IR). The samples were characterized by a Woolam IR-VASE ellipsometer equipped with programmable heating stage (Linkam Scientific).[59] The temperature was cycled between 30 and 100 °C with a rate of 5 °C min^{-1}, a rate of temperature change that is realistic for applications as paints and textile. Spectra were recorded between 7937 and 250 cm^{-1} and were acquired every 5 °C.

■ REFERENCES

(1) Maile, F. J.; Pfaff, G.; Reynders, P. Effect Pigments—Past, Present and Future. *Prog. Org. Coat.* 2005, 54, 150−163.

(2) Goerlitzer, E. S. A.; Klupp Taylor, R. N.; Vogel, N. Bioinspired Photonic Pigments from Colloidal Self-Assembly. *Adv. Mater.* 2018, 30, 1706654.

(3) Krishna, A.; Nie, X.; Warren, A. D.; Llorente-Bousquets, J. E.; Briscoe, A. D.; Lee, J. Infrared Optical and Thermal Properties of Microstructures in Butterfly Wings. *Proc. Natl. Acad. Sci.* 2020, 117, 1566−1572.

(4) Zhu, W.; Droguet, B.; Shen, Q.; Zhang, Y.; Parton, T. G.; Shan, X.; Parker, R. M.; De Volder, M. F. L.; Deng, T.; Vignolini, S.; Li, T. Structurally Colored Radiative Cooling Cellulosic Films. *Adv. Sci.* 2022, 9, 2202061.

(5) Wang, J.; Sultan, U.; Goerlitzer, E. S. A.; Mbah, C. F.; Engel, M.; Vogel, N. Structural Color of Colloidal Clusters as a Tool to Investigate Structure and Dynamics. *Adv. Funct. Mater.* 2020, 30, 1907730.

(6) Parker, R. M.; Zhao, T. H.; Frka-Petesic, B.; Vignolini, S. Cellulose Photonic Pigments. *Nat. Commun.* 2022, 13, 3378.

(7) Wang, Z.; Li, R.; Zhang, Y.; Chan, C. L. C.; Haataja, J. S.; Yu, K.; Parker, R. M.; Vignolini, S. Tuning the Color of Photonic Glass Pigments by Thermal Annealing. *Adv. Mater.* 2022, 2207923.

(8) Zhao, T. H.; Jacucci, G.; Chen, X.; Song, D.-P.; Vignolini, S.; Parker, R. M. Angular-Independent Photonic Pigments via the Controlled Micellization of Amphiphilic Bottlebrush Block Copolymers. *Adv. Mater.* 2020, 32, 2002681.

(9) Sakai, M.; Kim, H.; Arai, Y.; Teratani, T.; Kawai, Y.; Kuwahara, Y.; Abe, K.; Kuwana, Y.; Ikeda, K.; Yamada, K.; Takeoka, Y. Monodisperse Silica Nanoparticle−Carbon Black Composite Microspheres as Photonic Pigments. *ACS Appl. Nano Mater.* 2020, 3, 7047− 7056.

(10) Cencillo-Abad, P.; Franklin, D.; Mastranzo-Ortega, P.; Sanchez-Mondragon, J.; Chanda, D. Ultralight Plasmonic Structural Color Paint. *Sci. Adv.* 2023, 9, No. eadf7207.

(11) Avci, C.; De Marco, M. L.; Byun, C.; Perrin, J.; Scheel, M.; Boissière, C.; Faustini, M. Metal−Organic Framework Photonic Balls: Single Object Analysis for Local Thermal Probing. *Adv. Mater.* 2021, 33, 2104450.

(12) Wang, J.; Liu, Y.; Bleyer, G.; Goerlitzer, E. S. A.; Englisch, S.; Przybilla, T.; Mbah, C. F.; Engel, M.; Spiecker, E.; Imaz, I.; Maspoch, D.; Vogel, N. Coloration in Supraparticles Assembled from Polyhedral Metal-Organic Framework Particles. *Angew. Chem., Int. Ed.* 2022, 61, No. e202117455.

(13) Ming, S.; Zhang, X.; Chan, C. L. C.; Wang, Z.; Bay, M. M.; Parker, R. M.; Vignolini, S. Exploiting the Thermotropic Behavior of Hydroxypropyl Cellulose to Produce Edible Photonic Pigments. *Adv. Sustainable Syst.* 2023, 7, 2200469.

(14) Wenderoth, S.; Bleyer, G.; Endres, J.; Prieschl, J.; Vogel, N.; Wintzheimer, S.; Mandel, K. Spray-Dried Photonic Balls with a Disordered/Ordered Hybrid Structure for Shear-Stress Indication. *Small* 2022, 18, 2203068.

(15) Chehadi, Z.; Boissiere, C.; Chaneac, C.; Faustini, M. Nanoconfined water vapour as a probe to evaluate plasmonic heating. *Nanoscale* 2020, 12, 13368−13376.

(16) Odziomek, M.; Thorimbert, F.; Boissiere, C.; Drisko, G. L.; Parola, S.; Sanchez, C.; Faustini, M. Periodic Nanoporous Inorganic Patterns Directly Made by Self-Ordering of Cracks. *Adv. Mater.* 2022, 34, 2204489.

(17) Cui, Y.; Ke, Y.; Liu, C.; Chen, Z.; Wang, N.; Zhang, L.; Zhou, Y.; Wang, S.; Gao, Y.; Long, Y. Thermochromic VO$_2$ for Energy-Efficient Smart Windows. *Joule* 2018, 2, 1707−1746.

(18) Gonçalves, A.; Resende, J.; Marques, A. C.; Pinto, J. V.; Nunes, D.; Marie, A.; Goncalves, R.; Pereira, L.; Martins, R.; Fortunato, E. Smart Optically Active VO$_2$ Nanostructured Layers Applied in Roof-Type Ceramic Tiles for Energy Efficiency. *Sol. Energy Mater. Sol. Cells* 2016, 150, 1−9.

(19) Goodenough, J. B. The Two Components of the Crystallographic Transition in VO$_2$. *J. Solid State Chem.* 1971, 3, 490−500.

(20) Kumar, S.; Strachan, J. P.; Kilcoyne, A. L. D.; Tyliszczak, T.; Pickett, M. D.; Santori, C.; Gibson, G.; Williams, R. S. The Phase Transition in VO$_2$ Probed Using X-Ray, Visible and Infrared Radiations. *Appl. Phys. Lett.* 2016, 108, 073102.

(21) Christmann, T.; Felde, B.; Niessner, W.; Schalch, D.; Scharmann, A. Thermochromic VO$_2$ Thin Films Studied by Photoelectron Spectroscopy. *Thin Solid Films* 1996, 287, 134−138.

(22) Devthade, V.; Lee, S. Synthesis of Vanadium Dioxide Thin Films and Nanostructures. *J. Appl. Phys.* 2020, 128, 231101.

(23) Okimura, K.; Kubo, N. Growth of VO$_2$ Films with Metal-Insulator Transition on Silicon Substrates in Inductively Coupled Plasma-Assisted Sputtering. *Thin Solid Films* 2007, 515, 4992−4995.

(24) Béteille, F.; Mazerolles, L.; Livage, J. Microstructure and Metal-Insulating Transition of VO$_2$ Thin Films. *Mater. Res. Bull.* 1999, 34, 2177−2184.

(25) Li, S.; Li, Y.; Qian, K.; Ji, S.; Luo, H.; Gao, Y.; Jin, P. Functional Fiber Mats with Tunable Diffuse Reflectance Composed of Electrospun VO$_2$ /PVP Composite Fibers. *ACS Appl. Mater. Interfaces* 2014, 6, 9−13.

(26) Qian, K.; Li, S.; Ji, S.; Li, W.; Li, Y.; Chen, R.; Jin, P. Fabrication of VO2 Nanorods/PVP Composite Fiber Mats and Their Unique Optical Diffuse Reflectance Properties. *Ceram. Int.* 2014, 40, 14517− 14521.

(27) Saeli, M.; Piccirillo, C.; Parkin, I. P.; Ridley, I.; Binions, R. Nano-Composite Thermochromic Thin Films and Their Application in Energy-Efficient Glazing. *Sol. Energy Mater. Sol. Cells* 2010, 94, 141−151.

(28) Seyfouri, M. M.; Binions, R. Sol-Gel Approaches to Thermochromic Vanadium Dioxide Coating for Smart Glazing Application. *Sol. Energy Mater. Sol. Cells* 2017, 159, 52−65.

(29) Manning, T. D.; Parkin, I. P.; Pemble, M. E.; Sheel, D.; Vernardou, D. Intelligent Window Coatings: Atmospheric Pressure Chemical Vapor Deposition of Tungsten-Doped Vanadium Dioxide. *Chem. Mater.* 2004, 16, 744−749.

(30) Chang, T.; Cao, X.; Dedon, L. R.; Long, S.; Huang, A.; Shao, Z.; Li, N.; Luo, H.; Jin, P. Optical Design and Stability Study for Ultrahigh-Performance and Long-Lived Vanadium Dioxide-Based Thermochromic Coatings. *Nano Energy* 2018, 44, 256−264.

(31) Tadjer, M. J.; Wheeler, V. D.; Downey, B. P.; Robinson, Z. R.; Meyer, D. J.; Eddy, C. R.; Kub, F. J. Temperature and Electric Field Induced Metal-Insulator Transition in Atomic Layer Deposited VO$_2$ Thin Films. *Solid-State Electron.* 2017, 136, 30−35.

(32) Vernardou, D.; Louloudakis, D.; Spanakis, E.; Katsarakis, N.; Koudoumas, E. Amorphous Thermochromic VO$_2$ Coatings Grown by APCVD at Low Temperatures. *Adv. Mater. Lett.* 2015, 6, 660−663.

(33) Malarde, D.; Powell, M. J.; Quesada-Cabrera, R.; Wilson, R. L.; Carmalt, C. J.; Sankar, G.; Parkin, I. P.; Palgrave, R. G. Optimized Atmospheric-Pressure Chemical Vapor Deposition Thermochromic VO$_2$ Thin Films for Intelligent Window Applications. *ACS Omega* 2017, 2, 1040−1046.

(34) Ho, H.-C.; Lai, Y.-C.; Chen, K.; Dao, T. D.; Hsueh, C.-H.; Nagao, T. High Quality Thermochromic VO_2 Films Prepared by Magnetron Sputtering Using V_2O_5 Target with in Situ Annealing. *Appl. Surf. Sci.* **2019**, *495*, 143436.

(35) Juan, P.-C.; Lin, K.-C.; Lin, C.-L.; Tsai, C.-A.; Chen, Y.-C. Low Thermal Budget Annealing for Thermochromic VO_2 Thin Films Prepared by High Power Impulse Magnetron Sputtering. *Thin Solid Films* **2019**, *687*, 137443.

(36) Ashok, P.; Chauhan, Y. S.; Verma, A. High Infrared Reflectance Modulation in VO_2 Films Synthesized on Glass and ITO Coated Glass Substrates Using Atmospheric Oxidation of Vanadium. *Opt. Mater.* **2020**, *110*, 110438.

(37) Benkahoul, M.; Chaker, M.; Margot, J.; Haddad, E.; Kruzelecky, R.; Wong, B.; Jamroz, W.; Poinas, P. Thermochromic VO_2 Film Deposited on Al with Tunable Thermal Emissivity for Space Applications. *Sol. Energy Mater. Sol. Cells* **2011**, *95*, 3504−3508.

(38) Liu, C.; Cao, X.; Kamyshny, A.; Law, J. Y.; Magdassi, S.; Long, Y. VO_2/Si−Al Gel Nanocomposite Thermochromic Smart Foils: Largely Enhanced Luminous Transmittance and Solar Modulation. *J. Colloid Interface Sci.* **2014**, *427*, 49−53.

(39) Faustini, M. Sol−Gel Engineering to Tune Structural Colours. *J. Sol-Gel Sci. Technol.* **2020**, *95*, 504−516.

(40) Livage, J.; Henry, M.; Sanchez, C. Sol-Gel Chemistry of Transition Metal Oxides. *Prog. Solid State Chem.* **1988**, *18*, 259−341.

(41) Speck, K. R.; Hu, H. S.-W.; Murphy, R. A.; Potember, R. S. Vanadium Dioxide Films Grown from Vanadium Tetrakis(t-Butoxide) by the Sol-Gel Process. *MRS Proc.* **1988**, *121*, 667.

(42) Partlow, D. P.; Gurkovich, S. R.; Radford, K. C.; Denes, L. J. Switchable Vanadium Oxide Films by a Sol-gel Process. *J. Appl. Phys.* **1991**, *70*, 443−452.

(43) Cavanna, E.; Segaud, J. P.; Livage, J. Optical Switching of Au-Doped VO_2 Sol-Gel Films. *Mater. Res. Bull.* **1999**, *34*, 167−177.

(44) Boissiere, C.; Grosso, D.; Chaumonnot, A.; Nicole, L.; Sanchez, C. Aerosol Route to Functional Nanostructured Inorganic and Hybrid Porous Materials. *Adv. Mater.* **2011**, *23*, 599−623.

(45) Wan, C.; Zhang, Z.; Woolf, D.; Hessel, C. M.; Rensberg, J.; Hensley, J. M.; Xiao, Y.; Shahsafi, A.; Salman, J.; Richter, S.; Sun, Y.; Qazilbash, M. M.; Schmidt-Grund, R.; Ronning, C.; Ramanathan, S.; Kats, M. A. On the Optical Properties of Thin-Film Vanadium Dioxide from the Visible to the Far Infrared. *Ann. Phys.* **2019**, *531*, 1900188.

(46) Debecker, D. P.; Le Bras, S.; Boissière, C.; Chaumonnot, A.; Sanchez, C. Aerosol Processing: A Wind of Innovation in the Field of Advanced Heterogeneous Catalysts. *Chem. Soc. Rev.* **2018**, *47*, 4112−4155.

(47) Yamaguchi, I.; Manabe, T.; Tsuchiya, T.; Nakajima, T.; Sohma, M.; Kumagai, T. Preparation and Characterization of Epitaxial VO_2 Films on Sapphire Using Postepitaxial Topotaxy Route via Epitaxial V_2O_3 Films. *Jpn. J. Appl. Phys.* **2008**, *47*, 1022−1027.

(48) Odziomek, M.; Bahri, M.; Boissiere, C.; Sanchez, C.; Lassalle-Kaiser, B.; Zitolo, A.; Ersen, O.; Nowak, S.; Tard, C.; Giraud, M.; Faustini, M.; Peron, J. Aerosol Synthesis of Thermally Stable Porous Noble Metals and Alloys by Using Bi-Functional Templates. *Mater. Horiz.* **2020**, *7*, 541−550.

(49) De Marco, M. L.; Baaziz, W.; Sharna, S.; Devred, F.; Poleunis, C.; Chevillot-Biraud, A.; Nowak, S.; Haddad, R.; Odziomek, M.; Boissière, C.; Debecker, D. P.; Ersen, O.; Peron, J.; Faustini, M. High-Entropy-Alloy Nanocrystal Based Macro- and Mesoporous Materials. *ACS Nano* **2022**, *16*, 15837−15849.

(50) Schroden, R. C.; Al-Daous, M.; Blanford, C. F.; Stein, A. Optical Properties of Inverse Opal Photonic Crystals. *Chem. Mater.* **2002**, *14*, 3305−3315.

(51) Aguirre, C. I.; Reguera, E.; Stein, A. Tunable Colors in Opals and Inverse Opal Photonic Crystals. *Adv. Funct. Mater.* **2010**, *20*, 2565−2578.

(52) Alie, D.; Gedvilas, L.; Wang, Z.; Tenent, R.; Engtrakul, C.; Yan, Y.; Shaheen, S. E.; Dillon, A. C.; Ban, C. Direct Synthesis of Thermochromic VO_2 through Hydrothermal Reaction. *J. Solid State Chem.* **2014**, *212*, 237−241.

(53) Lee, K. W.; Kweon, J. J.; Lee, C. E.; Gedanken, A.; Ganesan, R. Infrared-Wave Number-Dependent Metal−Insulator Transition in Vanadium Dioxide Nanoparticles. *Appl. Phys. Lett.* **2010**, *96*, 243111.

(54) Valmalette, J.-C.; Gavarri, J.-R. High Efficiency Thermochromic $VO_2(R)$ Resulting from the Irreversible Transformation of $VO_2(B)$. *Mater. Sci. Eng., B* **1998**, *54*, 168−173.

(55) Salagram, M. Infrared Spectrum of VO_2^+ Entity in $K_2C_2O_4 \cdot H_2O$ Crystals. *Phys. Status Solidi A* **1988**, *105*, K161−K164.

(56) O'Dwyer, C.; Lavayen, V.; Newcomb, S. B.; Santa Ana, M. A.; Benavente, E.; González, G.; Sotomayor Torres, C. M. Vanadate Conformation Variations in Vanadium Pentoxide Nanostructures. *J. Electrochem. Soc.* **2007**, *154*, K29.

(57) Hatton, B.; Mishchenko, L.; Davis, S.; Sandhage, K. H.; Aizenberg, J. Assembly of Large-Area, Highly Ordered, Crack-Free Inverse Opal Films. *Proc. Natl. Acad. Sci.* **2010**, *107*, 10354−10359.

(58) Faustini, M.; Giraud, M.; Jones, D.; Rozière, J.; Dupont, M.; Porter, T. R.; Nowak, S.; Bahri, M.; Ersen, O.; Sanchez, C.; et al. Hierarchically structured ultraporous iridium-based materials: a novel catalyst architecture for proton exchange membrane water electrolyzers. *Adv. Energy Mater.* **2019**, *9*, 1802136.

(59) Gayrard, M.; Chancerel, F.; De Marco, M. L.; Naumenko, D.; Boissière, C.; Rozes, L.; Amenitsch, H.; Peron, J.; Cattoni, A.; Faustini, M. Block-Copolymers Enable Direct Reduction and Structuration of Noble Metal-Based Films. *Small* **2022**, *18*, 2104204.